

Structural investigation of PAP derivatives by CoMFA and CoMSIA reveals novel insight towards inhibition of Bcr-Abl oncoprotein

Amor A. San Juan ^{a,b,*}

^a Life Science Division, Korea Institute of Science and Technology, P.O. Box 131, Cheongryang, Seoul 130-650, South Korea

^b School of Science, University of Science and Technology 52 Eoeun-dong, Yuseong-gu, Daejeon 305-333, South Korea

Received 14 September 2006; received in revised form 6 March 2007; accepted 6 March 2007

Available online 12 March 2007

Abstract

Molecular modeling by 3D-QSAR comparative molecular field analysis (CoMFA) and comparative molecular similarity indices analysis (CoMSIA) were employed on a series of phenylaminopyrimidine-based (PAP) Bcr-Abl inhibitors. The chemical structures of 63 PAP analogues were aligned using a template extracted from the crystal structure of STI571 bound to Abl kinase. Subsequently, the structures built were divided into training and test sets that include 53 and 10 compounds, respectively. Statistical results showed that the 3D-QSAR models generated from CoMSIA were superior to CoMFA (CoMSIA; $q^2 = 0.66$, $r^2 = 0.94$, $N = 3$, $F = 139.09$, $r^2_{\text{pred}} = 0.64$ while CoMFA; $q^2 = 0.53$, $r^2 = 0.73$, $N = 3$, $F = 43.53$, $r^2_{\text{pred}} = 0.61$). Based on the contour interpretation, the attachment of hydrophobic and bulky groups to the phenyl and pyrrolidine (D- and E-ring of NS-187, respectively) along with highly electronegative groups around the D-ring are important structural features for the design of second-generation Bcr-Abl inhibitors. The generated models are predictive based on reproducible values of the predicted compared with experimental activities in the test set. Further, the complementary analysis of contour maps to the Bcr-Abl binding site suggested the anchor points for binding affinity.

© 2007 Published by Elsevier Inc.

Keywords: 3D-QSAR; Bcr-Abl agents; Chronic myelogenous leukemia; Drug design

1. Introduction

Annually, chronic myeloid leukemia (CML) affects 1–2 people per 100,000 and constitutes 15% of adult leukemia. The hallmark of CML is the *BCR-ABL* fusion gene which results from a reciprocal *t*(9;22) chromosomal translocation in a hematopoietic stem cell [1]. This oncogene encodes a chimer Bcr-Abl protein that activates the aberrant activity of Abl tyrosine kinase. Imatinib mesylate (STI571, Gleevec) is a breakthrough drug which targets the tyrosine kinase activity of Bcr-Abl [2–4]. The discovery of imatinib exemplified the successful development of rationally designed treatment for a specific cancer [5,6]. Crystallographic study shows the specific binding of STI571 to the inactive conformation of Abl kinase [7]. Further structural study suggests that Abl myristylation regulates an inactive Abl conformation while the loss of myristylation

switches Abl into an active state [8]. Consequently, the dynamic change in the activation loop of Abl kinase from the inactive towards the active state confers cellular activation [9].

Chronic myelogenous leukemia progresses in three stages: chronic, accelerated and blast [10]. The initial chronic phase can be characterized by the gradual expansion of myeloid cells with normal differentiation. Subsequently the disease may advance into an intermediate accelerated phase, characterized by the presence of undifferentiated blast cells in the blood and marrow. Ultimately, in blast crisis the cells become genetically unstable marked by widespread mutations in the *BCR-ABL* gene that eventually lead to drug resistance [11]. In the great majority of chronic phase CML patients, imatinib therapy has been successful. However, some patients develop resistance to the drug after several years of therapy [12,13]. Imatinib-resistance emerges as a result of the reactivation of Bcr-Abl kinase through overproduction or mutations [14]. More than 40 point mutations are not just clustered around the inhibitor-binding site, but are spread throughout the kinase domain of Bcr-Abl oncoprotein [11]. In CML patients, the most resistant mutant residues observed were Thr315Ile, Gly250Glu,

* Correspondence address: Life Science Division, Korea Institute of Science and Technology, P.O. Box 131, Cheongryang, Seoul 130-650, South Korea.

E-mail address: amor.san_juan@up.edu.ph.

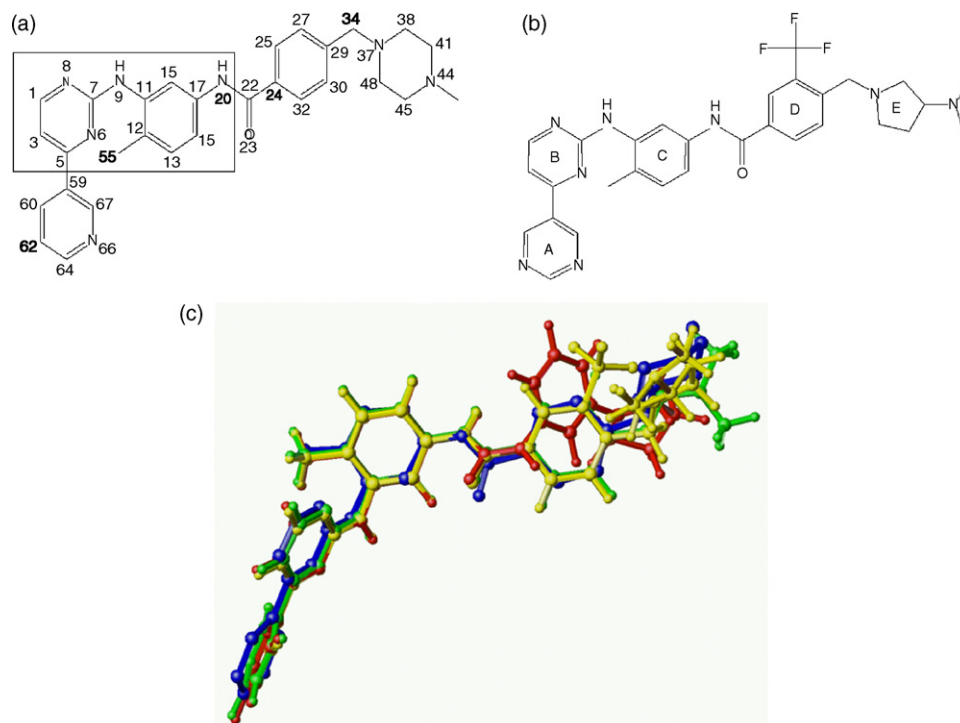


Fig. 1. (a) STI571 with atoms enclosed in the box are used as template for atom-fit, multi-fit and database alignments. (b) Chemical structure of the potent compound **61** (NS-187) shown with ring designations. (c) Superposition of conjugated STI571 active compounds: triazene (compound **43**, green), urea (compound **51**, red) and benzamide (compound **61**, yellow). The STI571 (compound **1**, blue) was obtained from the X-ray crystal structure (PDB entry 1OPJ).

Glu255Lys and Tyr253His [15]. These mutant amino-acid residues in the Abl kinase domain maintain the Bcr-Abl enzymatic activity but have a reduced binding affinity to imatinib [16].

The current focal point in CML research is the design and optimization of inhibitors active against resistant mutant residues. Overriding the resistance to imatinib can be classified into different inhibitors either as agents that target the pathways activated by *BCR-ABL*, agents that affect the stability of Bcr-Abl or agents alternative to Abl kinase [3]. Dasatinib (BMS-354825, Bristol-Myers Squibb) is a novel dual SRC/*BCR-ABL* kinase inhibitor that inhibits the majority of kinase mutations [17,18]. PD180970 (Parke-Davis) potently inhibits the autophosphorylation of p210^{Bcr-Abl} and induces apoptosis of blast crisis cell lines [19,20]. Nilotinib (AMN107, Novartis) is a high affinity inhibitor that targets many imatinib-resistant mutants of Bcr-Abl [21]. Recently, VX-680 (Vertex) demonstrates the ability to recognize and bind to an active conformation of Abl which effectively blocks Thr315 mutation [22]. Nevertheless, there are major drawbacks associated with the clinical use of these drugs. These include the resistance of dasatinib to mutant residue Thr315 and the low level of solubility as well as high cellular toxicity of PD180970 [18,23]. Hence, there is an urgent need to design second-generation Bcr-Abl agents.

Bcr-Abl inhibition by phenylaminopyrimidine (PAP) derivatives [24] has led to recent structurally related studies [25–27]. Structural modifications of STI571 (see Fig. 1a) at positions C₅₅ and N₂₀ by alkyl and triazene moieties,

respectively, yield the most potent compound **43** with an IC₅₀ value of 2 μM [25]. The replacement of amide in urea at position C₂₄ of STI571 yield compound **51** which showed better activity to both Bcr-Abl and c-Abl [26]. Recently, benzamide substitution at positions C₂₇ and C₂₉ of STI571 yielded a clinical candidate drug NS-187 (compound **61**, Fig. 1b) [27]. In Fig. 1c, the maximum overlap of compounds **43**, **51** and **61** with the X-ray crystal structure of STI571 [28] displays structural similarity of flexible molecules.

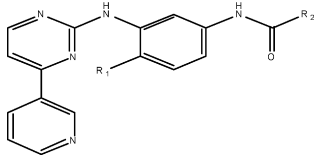
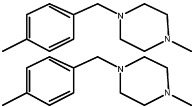
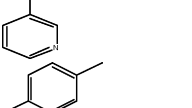
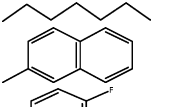
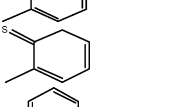
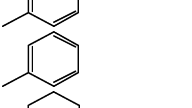
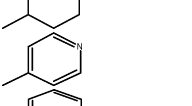
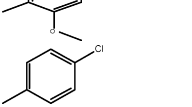
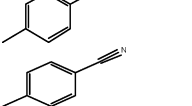
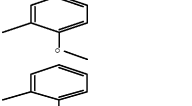
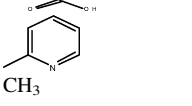

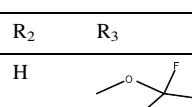
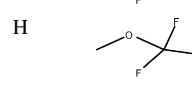


To date, this study is the first investigation to derive predictive 3D-QSAR models for Bcr-Abl tyrosine kinase. The present paper shows the molecular interactions of PAP derivatives with the active site of Bcr-Abl. Furthermore, this investigation determines the most essential structural properties for the design of new Bcr-Abl inhibitors.

2. Methodology

2.1. Data sets

Sixty-three PAP compounds were used as input data for 3D-QSAR analysis [24–27]. Table 1 shows the structures and potencies of these compounds. Manual selection of training (53 compounds) and test (10 compounds) sets was based on structural diversity and wide range of activity. The inhibition constant (IC₅₀) values, i.e., the concentration (nM) of inhibitor required for 50% inhibition to Bcr-Abl were converted into pIC₅₀ (–log IC₅₀) and subsequently used as dependent variables for CoMFA and CoMSIA analysis.

Table 1
Dataset structure and experimental activity

Compound			pIC ₅₀
	R ₁	R ₂	
1	CH ₃		7.42
2	H		7.00
3	H		6.82
4	CH ₃		6.70
5	H		6.70
6	CH ₃		6.70
7	H		6.70
8	H		6.52
9	H		6.40
10	CH ₃		6.40
11	H		6.35
12	H		6.30
13	CH ₃		6.10
14	CH ₃		6.10
15	H		6.00
16	H		5.89
17	H		5.72
18	H		5.70
19	H		5.42
20	CH ₃	CH ₃	5.24

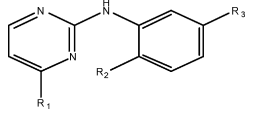
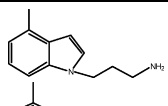
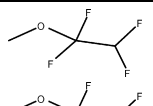
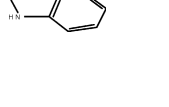
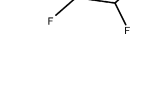
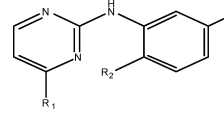
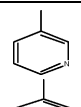
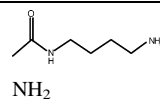
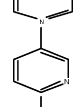
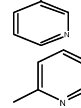
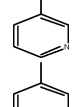
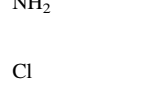
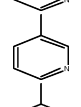
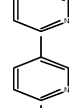
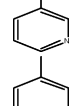
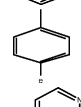
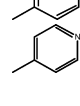
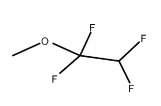
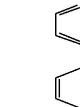

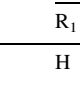
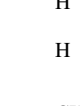
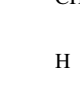
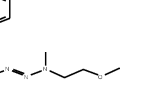
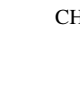


Compound				pIC ₅₀
	R ₁	R ₂	R ₃	
21		H		6.46
22		H		6.43

Table 1 (Continued)

Compound				pIC ₅₀
	R ₁	R ₂	R ₃	
23		H		6.40
24		H	NH ₂	6.22
25		H	NH ₂	6.15
26		H		6.00
27		H	NO ₂	5.92
28		CH ₃	NH ₂	5.82
29		H	Cl	5.82
30		H	H	5.74
31		H		5.48
32		H		5.29
33		H	COOH	5.10
34		H	NO ₂	4.47
35		H		4.30
36		H	NO ₂	4.21
37		H		4.00

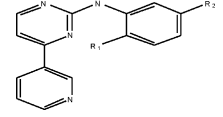
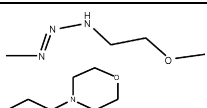
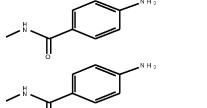
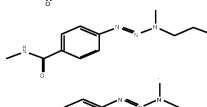
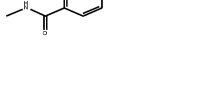

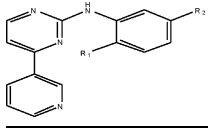
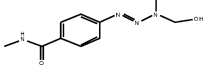
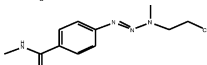
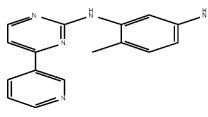
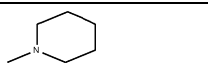
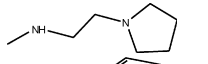
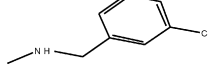
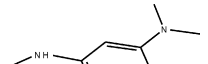
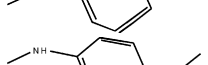
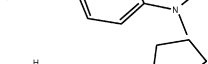
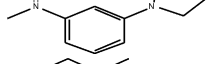
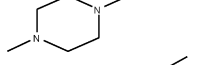
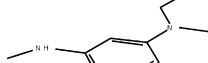
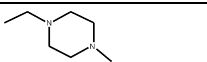
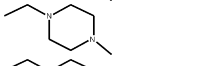
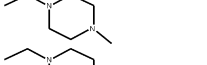
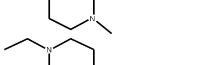
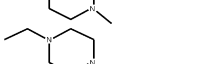
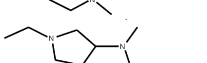
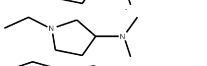
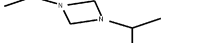
Compound				pIC ₅₀
	R ₁	R ₂		
38	H			5.27
39	H			5.00
40	H			5.01
41	CH ₃			4.17
42	H			4.79
43	CH ₃			5.66

Table 1 (Continued)

Compound				pIC ₅₀
	R ₁	R ₂		
44	CH ₃			5.50
45	CH ₃			4.76
Compound				pIC ₅₀
46				5.00
47				5.05
48				6.00
49				6.24
50				5.00
51				6.14
52				5.30
53				6.00
54				5.00
Compound	X	R ₁	R ₂	pIC ₅₀
55	CH	F		7.20
56	CH	Cl		8.00
57	CH	Br		8.15
58	CH	I		8.00
59	CH	CF ₃		8.30
60	N	CF ₃		8.40
61	N	CF ₃		8.40
62	N	CF ₃		7.96
63	N	CF ₃		7.77

2.2. Molecular modelling

Molecular modeling calculations were performed by SYBYL v7.2 on a Silicon Graphics Octane (R1200) workstation with an IRIX 6.5 operating system [29]. The chemical structures of the compounds were built by employing the Sketch option in SYBYL. All structures were minimized by using the Tripos force field [30] and Gasteiger–Huckel charges. Geometry optimization of the compounds was carried out by removing the constraints using conjugate gradient with a convergence criterion of 0.005 kcal mol⁻¹.

2.3. CoMFA and CoMSIA

Comparative molecular field analysis (CoMFA) models of steric and electrostatic fields were based on Lennard-Jones and Coulomb potentials, respectively [31]. The CoMFA was performed to evaluate the steric and electrostatic properties associated with the activity of compounds. Initially, a three-dimensional cubic lattice with 2 Å grid spacing was generated automatically around the molecules to ensure that the grid extended the molecular dimensions by 4 Å in all directions. Next, the steric and electrostatic field energies were calculated using an sp³ carbon probe with van der Waals radius of 1.52 Å and a +1 charge. Energies were truncated to ±30 kcal mol⁻¹ and the electrostatic contribution was ignored at lattice points with maximum steric interactions. Finally, the CoMFA fields automatically generated were block scaled by the CoMFA standard method in SYBYL. In a CoMFA study, the selection of the bioactive conformation is essential [32]. The available crystal structure of compound 1 (STI571) was extracted from the co-crystallized protein structure (PDB code: 1OPJ) [28] and subsequently used as template to align all compounds in the dataset. The fifteen common atoms of the template were used to superimpose the compounds (Fig. 1a, atoms inside the rectangular box). Three different alignment methods such as atom-fit, database, and multi-fit were carried out.

Comparative molecular similarity index analysis (CoMSIA) was employed to determine the hydrophobic and hydrogen-bond properties related with the activity of compounds [33]. CoMSIA descriptors were derived by the same lattice box used for the CoMFA calculations. All five CoMSIA similarity index fields (steric, electrostatic, hydrophobic, hydrogen bond donor, and hydrogen bond acceptor) were evaluated using the sp³ carbon probe. The CoMSIA models from hydrophobic and hydrogen bonds were calculated between the grid point and each atom of the molecule by a Gaussian function [33]. The implementation of a Gaussian distance function generates smoother sampling of the descriptor fields around the molecules. Similarly to the CoMFA study, a data table was constructed from similarity indices calculated at the intersections of a regularly spaced lattice with 2 Å spacing [33,34]. Similarity indices $A_{F,k}$ between the compounds of interest and a

probe atom were calculated [33] according to the equation below.

$$A_{F,k^q(j)} = \sum_{i=1}^n w_{\text{probe},k} w_{ik} e^{-\alpha r_{iq}^2}$$

In this equation, q is the grid point of the molecule j , with i the summation index over all atoms of the molecule j , w_{ik} the actual value of physicochemical property k of atom i , $w_{\text{probe},k}$ indicates probe atom with charge of +1, radius of 1 Å, hydrophobicity of +1, hydrogen bond donor and acceptor properties of +1, α is the attenuation factor; and r_{iq} is the mutual distance between the

probe atom at grid point q and atom i of the test molecule. A standard attenuation factor of $\alpha = 0.30$ generates a contour map with prominent molecular features. In contrast, a higher value of the attenuation factor results to less molecular features due to a steeper Gaussian function. The present study employed a value of $\alpha = 0.50$ to obtain localized and detailed polyhedra.

2.4. Partial least square (PLS) and model validations

Initial PLS regression analysis for CoMFA and CoMSIA were obtained from leave-one-out cross-validation [35]. In this

Table 2
Summary of results by CoMFA and CoMSIA studies on Bcr-Abl inhibitors

PLS results		CoMFA alignment						
		Atom-fit		Multi-fit		Database		
q^{2a}		0.53		0.39		0.41		
N^b		3		4		3		
r^{2c}		0.73		0.80		0.75		
SEE ^d		0.59		0.50		0.57		
F -value ^e		43.53		66.90		47.78		
$r^2_{\text{pred}}{}^f$		0.61		0.63		0.66		
Contributions ^g		0.55, 0.45		0.38, 0.62		0.50, 0.50		
PLS results		CoMSIA fields						
		SE	SHE	SED	SEA	SEDA	SEHD	SEHDA
Atom-fit								
q^{2a}		0.56	0.55	0.66	0.57	0.69	0.65	0.66
N^b		4	1	5	4	8	7	8
r^{2c}		0.87	0.64	0.94	0.88	0.99	0.98	0.99
SEE ^d		0.42	0.66	0.29	0.40	0.14	0.16	0.14
F -value ^e		77.40	90.39	139.09	85.99	394.03	295.89	368.29
$r^2_{\text{pred}}{}^f$		0.54	0.69	0.64	0.54	0.61	0.55	0.57
Contributions ^g		0.33, 0.67	0.24, 0.37	0.25, 0.47	0.29, 0.52	0.21, 0.38	0.15, 0.36	0.14, 0.28
			0.40	0.28	0.20	0.22, 0.18	0.31, 0.19	0.26,0.18,0.14
Multi-fit								
q^{2a}		0.31	0.26	0.46	0.37	0.50	0.39	0.44
N^b		4	2	6	3	10	7	10
r^{2c}		0.78	0.71	0.90	0.82	0.99	0.97	0.99
SEE ^d		0.52	0.60	0.37	0.47	0.13	0.20	0.11
F -value ^e		59.22	60.78	103.40	74.80	361.65	220.54	502.36
$r^2_{\text{pred}}{}^f$		0.60	0.67	0.71	0.49	0.75	0.73	0.78
Contributions ^g		0.36, 0.64	0.24, 0.41	0.20, 0.39	0.22, 0.39	0.15, 0.30	0.14, 0.297	0.11, 0.22
			0.35	0.41	0.39	0.28, 0.27	0.24, 0.32	0.20,0.24,0.22
Database								
q^{2a}		0.52	0.49	0.45	0.47	0.45	0.49	0.46
N^b		3	2	3	3	4	3	3
r^{2c}		0.77	0.72	0.81	0.78	0.85	0.81	0.79
SEE ^d		0.53	0.59	0.50	0.52	0.44	0.49	0.52
F -value ^e		64.67	64.45	50.63	58.38	68.09	68.90	60.55
$r^2_{\text{pred}}{}^f$		0.79	0.69	0.62	0.62	0.58	0.66	0.66
Contributions ^g		0.46, 0.54	0.27, 0.33	0.34, 0.40	0.32, 0.40	0.26, 0.31	0.22, 0.27	0.19, 0.23
			0.39	0.26	0.28	0.23, 0.20	0.31, 0.20	0.28,0.17,0.14

^a Cross-validated correlation coefficient.

^b Optimum number of components.

^c Non-cross-validated correlation coefficient.

^d Standard error of estimate.

^e F -test value.

^f Predictive r^2 .

^g Field contributions: S, steric; E, electrostatic; H, hydrophobic; D, hydrogen bond donor; A, hydrogen bond acceptor.

technique, compounds are excluded from the data set, and the activity of each removed compound is predicted by a new model derived from the remaining compounds in the set. Column filtering thresholds of 2.0 kcal mol⁻¹ for CoMFA and 1.0 kcal mol⁻¹ for CoMSIA were employed to shorten the computational time and to reduce the background noise. The final non-cross-validated analysis was performed by using the optimal number of components previously determined from cross-validation [36,37].

Two validation methods that consist of statistical correlations and docking analysis were carried out to evaluate the predictive ability of the generated models. First, the cross-validated q^2 and conventional correlation coefficient r^2 were calculated based on the overall compounds in the training set while predictive r^2 (r^2_{pred}) was calculated overall for the test set. Predictive r^2 validates the model obtained from CoMFA and CoMSIA by evaluating the correlation between actual and predicted inhibition of the test set using the model derived from the training set [38]. Second, molecular docking was performed to check the consistency between the contour maps and the binding site. Docking was reported to be useful in validating the 3D-QSAR results [39–41]. In this study, FlexX interfaced with the SYBYL was employed in the docking analysis [42]. FlexX is a fast and automated program that considers ligand conformational flexibility by an incremental fragment placing technique [42,43]. Initially, the ligand and protein coordinates were prepared. The charges of the ligands were removed and replaced by formal charges. The ligand and water molecules were removed from the 2F4J [44] protein structure and subsequently added with hydrogen atoms and the Kollman-all atom charges. Next, the active site for docking was selected for residues located within a distance of 6.5 Å from the co-crystallized ligand. Charged residues located at the binding site were protonated and ionized at the physiological pH of 7.0. Redocking the bound crystal structure of the ligand to its active site validated the reliability of FlexX. The low root-mean-square-deviation of 0.71 Å for the inhibitor–protein complex VX680-2F4J indicates reproducibility of the docked complex and hence the reliability of FlexX.

3. Results and discussion

3.1. 3D-QSAR CoMFA and CoMSIA models

Table 2 shows the PLS obtained from three different alignment methods. Atom-fit yields the highest cross-validated q^2 value of 0.53 in contrast with database (0.41) and multi-fit (0.39) methods. While the conventional r^2 values for database and atom-fit were found nearly equivalent (0.73 and 0.75, respectively), the multi-fit gave the highest r^2 value of 0.80. Predictive r^2 is slightly lower in case of atom-fit as compared with database and multi-fit. The robustness of atom-fit from CoMFA is in agreement with the CoMSIA analysis of steric and electrostatic fields. Based on the above observations atom-fit was chosen for further analysis.

Several statistical parameters such as q^2 , r^2 , N , r^2_{pred} and F were used to evaluate the robustness of a QSAR model. High coefficient values (>0.50) for the three standard squared correlations: r^2 , q^2 , and r^2_{pred} indicate a good quality QSAR model. Firstly, consideration was based on high q^2 at the optimum number of components. The best models include CoMFA (SE: steric, electrostatic) and CoMSIA (SED: steric, electrostatic, hydrogen-bond donor). Although the other CoMSIA combination of SEDA (steric, electrostatic, hydrogen bond donor and acceptor) and SEHDA (all descriptors) showed relatively higher values of q^2 and r^2 , their principal components were too high. Thus, it appears that the steric, electrostatic and hydrogen bond donor fields are essential for Bcr-Abl activity. Next, let us consider which models are best based on high r^2_{pred} values. Tropsha [45] emphasized that a high q^2 value (>0.50) is a necessary but not sufficient condition for a predictive QSAR model. Therefore, once models with low q^2 , low r^2 and high N values were ruled out, the best models should be chosen based on high r^2_{pred} [45]. Almost all the models performed well ($r^2_{\text{pred}} > 0.50$) in the activity prediction of test compounds (Table 2). Further, the predicted pIC₅₀ values were close to the observed values with residuals no larger than one log unit (Table 3). The r^2_{pred} values of CoMSIA models such as steric, electrostatic, hydrophobic (SEH) and SED were much higher

Table 3
Comparison between the predicted and experimental activities used in the test set for CoMFA^a and CoMSIA^b

Compound	IC ₅₀ (nM)	Actual pIC ₅₀	CoMFA		CoMSIA	
			Predicted pIC ₅₀	Residual ^c	Predicted pIC ₅₀	Residual ^c
4	200	6.70	5.83	0.87	6.11	0.59
12	500	6.30	5.85	0.45	5.98	0.32
15	1000	6.00	5.89	0.11	6.33	−0.33
20	5800	5.24	5.69	−0.45	6.19	−0.95
35	50000	4.30	5.61	−1.31	5.45	−1.15
44	3151	5.50	5.11	0.39	5.60	−0.10
48	1003	6.00	5.55	0.45	5.82	0.18
53	1000	6.00	5.41	0.59	6.07	−0.07
55	63	7.20	7.64	−0.44	8.02	−0.82
57	7	8.15	7.67	0.48	7.89	0.26

^a Atom fit alignment.

^b Using steric, electrostatic and donor fields.

^c Difference of results obtained by actual and predicted values.

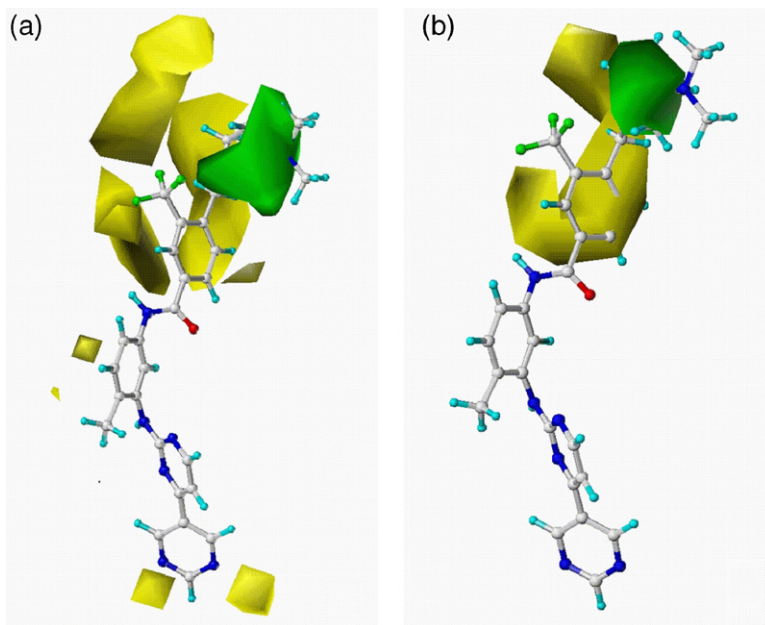


Fig. 2. Steric field contour map (a) CoMFA and (b) CoMSIA) around the potent compound **61** (shown in ball-and-stick). Green (yellow) regions indicate where bulky groups increase (decrease) the Bcr-Abl activity. (For interpretation of the references to colour in this figure legend, the reader is referred to the web version of the article.)

than for the rest of the models considered. The relatively higher value of q^2 than r^2_{pred} in the SED model may imply that the model predictability outweighs the overall predictive performance. Overall, based on q^2 , r^2 , r^2_{pred} , N as well as the highest value of the Fisher F -test, the best models include the SE fields from CoMFA as well as the SEH and SED fields from CoMSIA. Thus, the models included in the graphical analysis were the steric, electrostatic, hydrophobic and hydrogen bond donor fields. These graphical contour maps could be selected and used

as the final screening tool for lead optimization in designing new Bcr-Abl agents.

3.2. Contour maps

3.2.1. Steric field

Fig. 2 shows the steric contours from CoMFA and CoMSIA. Green polyhedra represent a steric group that confers an increased affinity while yellow polyhedra represent a bulky

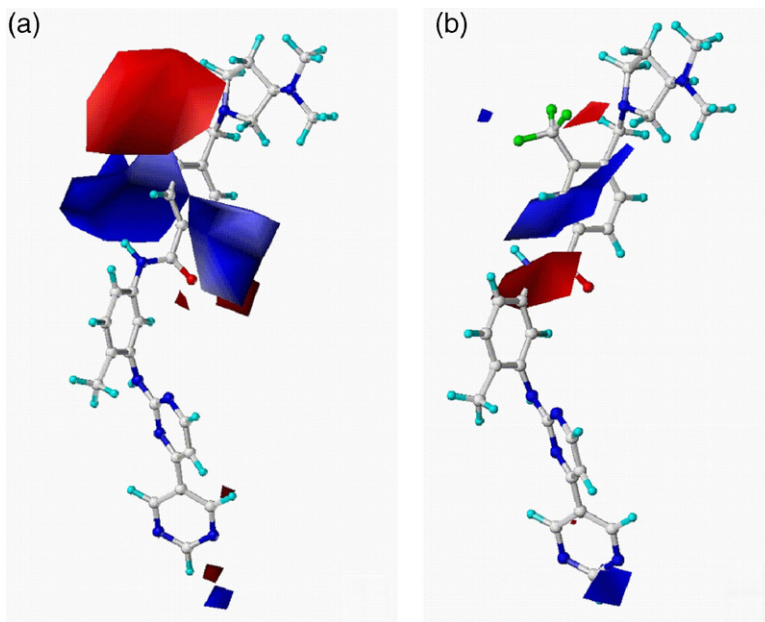


Fig. 3. Electrostatic field contour map (a) CoMFA and (b) CoMSIA) around the potent compound **61** rendered in ball-and-stick model. Red (blue) regions indicate where electronegative groups increase (decrease) the Bcr-Abl activity. (For interpretation of the references to colour in this figure legend, the reader is referred to the web version of the article.)

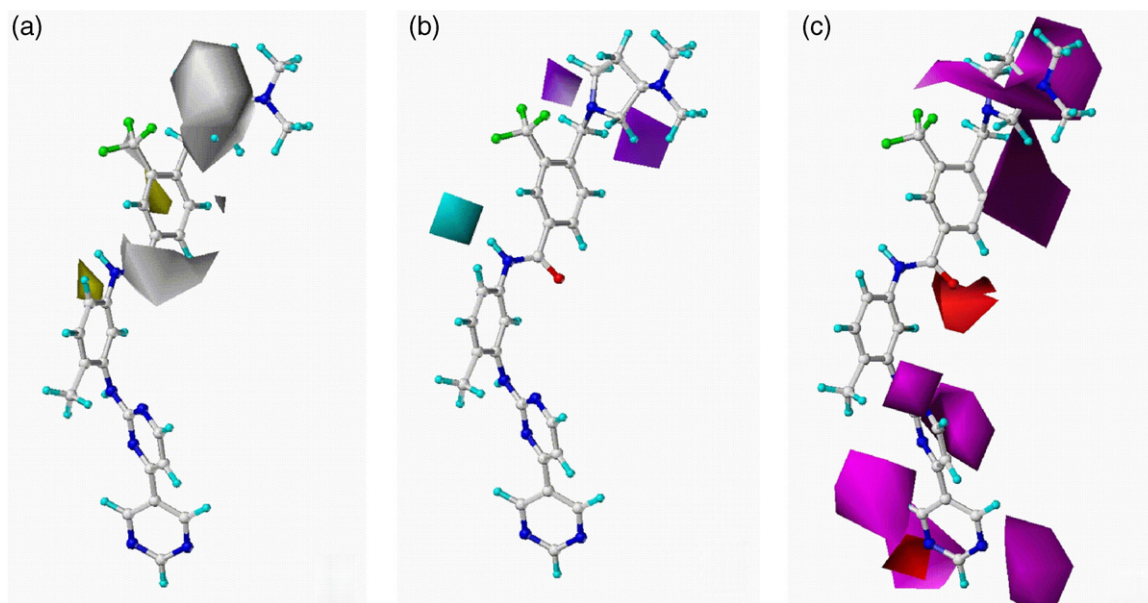


Fig. 4. CoMSIA contour plots (a) hydrophobic fields (yellow, favored; white, disfavored), (b) hydrogen bond donor fields (cyan, favored; purple, disfavored), and (c) hydrogen bond acceptor (magenta, favored; red, disfavored). The CoMSIA contour maps surround the potent compound **61** rendered in ball-and-stick model.

group that results in a decreased affinity. The CoMSIA steric contour appeared more localized and detailed in marked contrast with CoMFA fields. Except for differences in the polyhedron volume, the steric contours for CoMFA and CoMSIA indicate a consensus that bulky substituents on the E-ring (refer to Fig. 1b) will improve activity. This can be explained by analyzing the structural features and biological activities of compounds **60–63**. The replacement of the piperazine moiety in STI571 with pyrrolidine (**61**) showed comparable activity. However, the substituted azetidine (**63**) decreased the activity by four-fold. Further, the attachment of a pyrrolidine moiety in compounds **55–63** showed higher activities as compared to an additional linker between the C- and D-rings (compounds **46–54**). In contrast, the comparison of compounds **1–19** and **55–63** with less active compounds **39–45** indicated that the replacement of benzene by triazene did not favor the activity. The additional attachment of benzene to the D-ring showed improved activities as shown by compounds

1–19 and **55–63** but less inhibitory activities for compounds **39–45**. This is best attributed to the hydrophobic property of conjugated triazene with benzene (see hydrophobic field). The small yellow blocks located at the *meta*-position of the C-ring and further two yellow blocks near the A-ring suggested unfavorable steric group substitution. To illustrate this, the compounds with bulky indole group in the A-ring exhibited by compounds **21** and **22** showed decreased activities while compounds with six-membered ring showed improved activities.

3.2.2. Electrostatic field

The electrostatic contour maps of CoMFA and CoMSIA were found to be consistent with each other (Fig. 3). A red contour indicates that an electronegative group will favor the activity while a blue contour will reduce the activity. In CoMFA, a small red block found in between the amide and D-ring is particularly located at the amide position in CoMSIA.

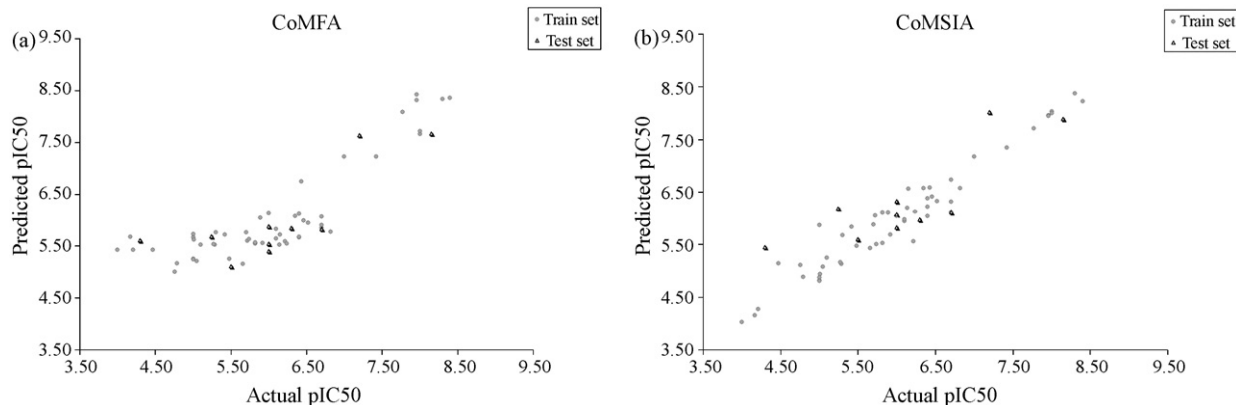


Fig. 5. (a) The correlation ($r^2 = 0.71$) between experimental and predicted pIC_{50} s for training and test sets obtained from CoMFA. (b) The correlation ($r^2 = 0.90$) between experimental and predicted pIC_{50} s for training and test sets obtained from CoMSIA.

Table 4

Comparison between the predicted and experimental activities used in the training set for CoMFA^a and CoMSIA^b models

Compound	IC ₅₀ (nM)	Actual pIC ₅₀	CoMFA		CoMSIA	
			Predicted pIC ₅₀	Residual ^c	Predicted	Residual ^c pIC ₅₀
1	38	7.42	7.22	0.20	7.35	0.07
2	100	7.00	7.22	−0.22	7.17	−0.17
3	150	6.82	5.78	1.04	6.57	0.25
5	200	6.70	6.07	0.63	6.74	−0.04
6	200	6.70	5.85	0.85	6.32	0.38
7	200	6.70	5.91	0.79	6.11	0.59
8	300	6.52	5.95	0.57	6.33	0.19
9	400	6.40	5.67	0.73	6.22	0.18
10	400	6.40	5.68	0.72	6.04	0.36
11	450	6.35	6.08	0.27	6.58	−0.23
13	800	6.10	5.64	0.46	5.94	0.16
14	800	6.10	5.83	0.27	5.97	0.13
16	1300	5.89	6.05	−0.16	6.10	−0.21
17	1900	5.72	5.60	0.12	6.05	−0.33
18	2000	5.70	5.77	−0.07	5.88	−0.18
19	3800	5.42	5.72	−0.30	5.84	−0.42
21	350	6.46	5.99	0.47	6.41	0.05
22	370	6.43	6.74	−0.31	6.59	−0.16
23	400	6.40	6.12	0.28	6.38	0.02
24	600	6.22	5.59	0.63	5.56	0.66
25	700	6.15	5.72	0.43	6.56	−0.41
26	1000	6.00	6.13	−0.13	6.04	−0.04
27	1200	5.92	5.56	0.36	5.69	0.23
28	1500	5.82	5.55	0.27	6.10	−0.28
29	1500	5.82	5.57	0.25	5.52	0.30
30	1800	5.74	5.63	0.11	5.50	0.24
31	3300	5.48	5.25	0.23	5.47	0.01
32	5100	5.29	5.53	−0.24	5.13	0.16
33	8000	5.10	5.52	−0.42	5.25	−0.15
34	34000	4.47	5.43	−0.96	5.14	−0.67
36	61000	4.21	5.43	−1.22	4.27	−0.06
37	100000	4.00	5.43	−1.43	4.03	−0.03
38	5390	5.27	5.54	−0.27	5.16	0.11
39	10110	5.00	5.67	−0.67	4.82	0.18
40	9880	5.01	5.62	−0.61	4.94	0.07
41	68000	4.17	5.68	−1.51	4.15	0.02
42	16180	4.79	5.17	−0.38	4.88	−0.09
43	2164	5.66	5.15	0.51	5.43	0.23
45	17350	4.76	5.00	−0.24	5.11	−0.35
46	10000	5.00	5.73	−0.73	5.87	−0.87
47	9000	5.05	5.21	−0.16	5.08	−0.03
49	573	6.24	5.55	0.69	6.13	0.11
50	10000	5.00	5.25	−0.25	4.87	0.13
51	720	6.14	5.53	0.61	6.20	−0.06
52	5000	5.30	5.77	−0.47	5.67	−0.37
54	10000	5.00	5.24	−0.24	4.81	0.19
56	10	8.00	7.66	0.34	8.03	−0.03
58	10	8.00	7.71	0.29	8.00	0.00
59	5	8.30	8.33	−0.03	8.37	−0.07
60	4	8.40	8.36	0.04	8.23	0.17
61	4	8.40	8.31	0.09	7.96	0.44
62	11	7.96	8.42	−0.46	7.95	0.01
63	17	7.77	8.08	−0.31	7.71	0.06

^a Atom fit alignment.^b Using steric, electrostatic and donor fields.^c Difference of results obtained by actual and predicted values.

Moreover, a big red block encompassing the D- and E-rings in CoMFA corresponds to a small red block near the trifluoromethyl group in CoMSIA. The electronegative groups such as amide and trifluoromethyl indicated favored activity. For

example, compounds **1–15** and **55–63** with an amide bond showed improved activities while compounds **27–37** without an amide bond showed decreased activities. Further in the CoMFA map, there is a red block close to the *para*- or *meta*-position of

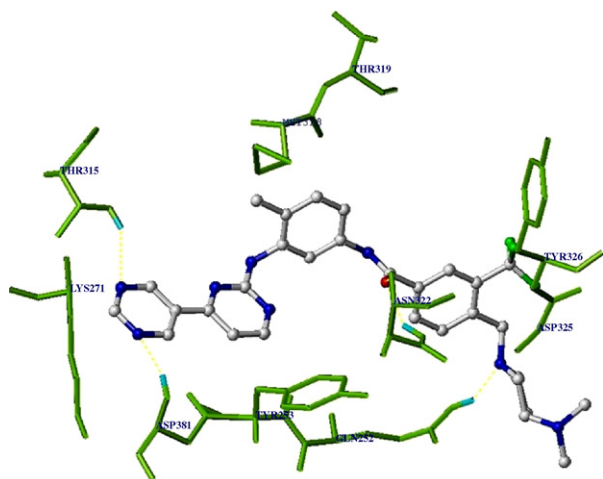


Fig. 6. Ligand-protein contact of compound **61** bound to Bcr-Abl oncoprotein (PDB ID: 2F4J). Four hydrogen bonds (shown in yellow dotted lines) were mediated in Gln252, Thr315, Asn322 and Asp381 residues of the active site.

the A-ring and a blue block just a little further away. This interpretation can be verified by the greater activity of compound **63** as compared with **59** that favors substitution of an electronegative atom at the *meta*-position of the A-ring. Otherwise in CoMSIA, a large blue block distinctly located at the *para*-position of the A-ring indicated improved activity by an electropositive group.

3.2.3. Hydrophobic field

Fig. 4a shows the hydrophobic contour obtained from CoMSIA steric, electrostatic and hydrophobic fields. The yellow contour suggests that a hydrophobic group favors the Bcr-Abl activity while a white contour reduces activity. The hydrophobic group located at the *meta*-position of the D-ring showed increased activity. The presence of a bulky group at the *meta*-position of the D-ring that is attached to hydrophilic elements such as CF₃: **59**; I: **58**; and F: **55** all showed good

activities (pIC_{50} = 8.30, 8.00, and 7.20, respectively). A big white block that covers the D- and E-rings indicates that a large hydrophobic group would decrease the activity. For example, compounds with one- or two-carbon linkers (**42–45**, **47–51**, **53–54**) were found to have relatively low activities.

3.2.4. Hydrogen bond donor and acceptor fields

The graphical interpretations of the field contributions for the hydrogen-bonding properties are shown in Fig. 4b (hydrogen-bond donor) and Fig. 4c (hydrogen-bond acceptor). A cyan isopleth around the amide indicates that a hydrogen-bond donor favors activity. In consequence, the nitration of amide in **34** showed decreased activity by 38-fold as compared with amination in **25**. The purple regions that surround the pyrrolidine indicate that the presence of a hydrogen-bond donor would reduce the affinity. This could explain that the compounds with a dimethylamino substituent in pyrrolidine (**61–62**) showed less potency than those without a substituent at this position (**59–60**). On the other hand, the magenta contours suggest a favorable hydrogen-bond acceptor. As a result the activity increased when pyridine was replaced by pyrimidine from compound **59** into **60**. The same region had been indicated in the electrostatic map (Fig. 3a) to favor a more electronegative charged group.

3.3. Model validations

Model validation examines the internal predictive power of the model and its ability to reproduce biological activities of the compounds. The quantitative (r^2_{pred}) and qualitative (molecular docking) evaluations were the tools used in validation. The computed affinities from the CoMFA and CoMSIA showed good correlation with experimental affinities (Fig. 5a and b, Tables 3 and 4). Furthermore, good predictive r^2 values of 0.61 (CoMFA) and 0.69 (best CoMSIA) suggest that the models were predictive. In addition to r^2_{pred} , docking was employed to

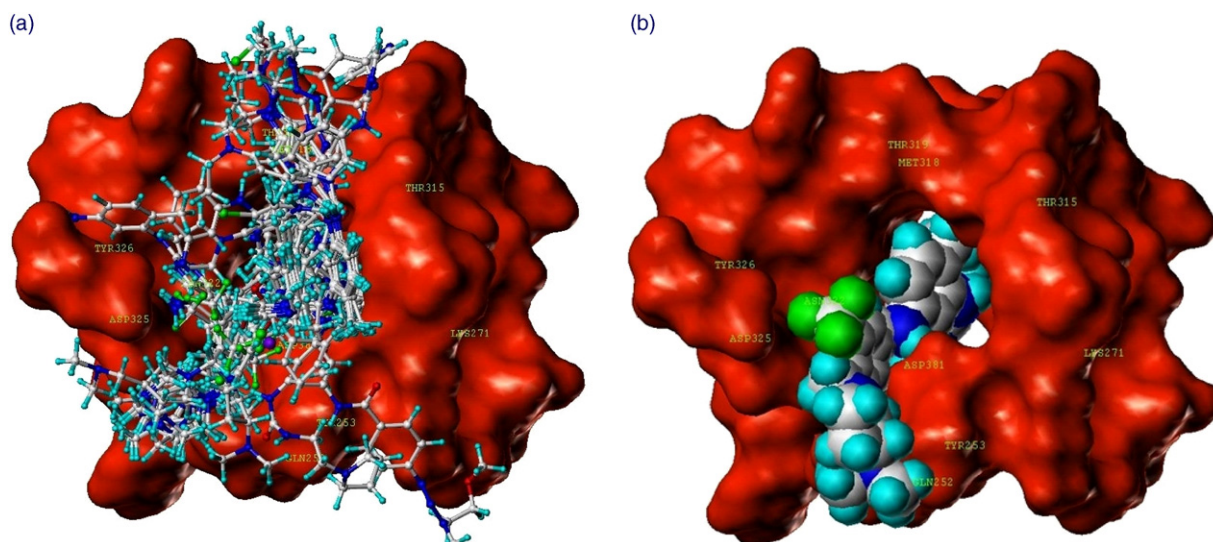


Fig. 7. (a) FlexX molecular docking of PAP inhibitors into the Bcr-Abl active site that shows the mode of binding on the Connolly solvent accessible surface with labels of amino acid residues. (b) Molecular docking of the most potent compound **61** (space-fill render) into the Bcr-Abl active site.

validate the reliability of the models. The consistency between the 3D-QSAR contour maps and the complementary features of PAP analogues with the binding site of Bcr-Abl indicates a unified pharmacophore model. A green isopleth (Fig. 2) that occupied the pyrrolidine of compound **61** was located near the slightly hydrophobic residue Lys245 (Fig. 6). Groups of increasing negative charge coincide with regions surrounded by red contours (Fig. 3). In this case, the two nitrogen atoms in pyrrolidine formed hydrogen bonds with Thr315 and Asp381 charged residues. Further, the red contour near the trifluoromethyl substituent was found to be projected along the hydrophilic pocket formed by the side chain residues Tyr326 and Asp325. Thus, a combination of electronegative groups with hydrophilic or aliphatic residues favored the interaction. Yellow contours (Fig. 4a) near the C- and D-rings which indicated the preference for hydrophobic group were found buried along the corresponding hydrophobic residues (Met318 and Thr319). Accordingly, the magenta contours (Fig. 4b) located in the pyrrolidine and carbonyl groups intuitively suggest the presence of hydrogen-bond donor groups at the active site which coincides with the hydrogen-bond contacts with Thr315, Asp381 and Asn322 residues. Overall, the hydrophobic surface of compound **61** was found in contact with the hydrophobic pocket of the receptor while the hydrophilic part was buried inside the cavity with charged residues. The docking analysis revealed insights of the molecular interaction of PAP analogues towards the active site of Bcr-Abl oncoprotein. Interestingly, few outlier compounds were found lying outside the active site (Fig. 7a as compared with b), suggesting that FlexX docking accuracy was affected by the diversity of the size and polarity of the ligands.

3.4. Discussion of related structural modeling study

Wisniewski et al. [20] performed biochemical assay and computational modeling of a PD series of compounds to the active conformation of Abl kinase. To explain structurally the higher activity of PD166326 as compared with PD173955, they employed manual docking to the active Abl kinase domain. The basis of comparison between the results from this study with their work should be qualified by the consideration that the models were fitted to Bcr-Abl kinase inhibition data. The putative binding conformation adopted in our study is quite similar to their docked conformation [20]. However, their modeling approach was limited by employing a single compound docked to active Abl kinase. The advantage of this present 3D-QSAR study is that a large dataset of diverse Bcr-Abl inhibitors were virtually screened for their molecular affinity in terms of steric, hydrophobic and hydrogen bonding physicochemical profiles.

4. Conclusion

Robust 3D-QSAR model inhibitors were established which revealed novel insights towards inhibition of Bcr-Abl oncoprotein. Structural replacements by larger substituents to pyrrolidine ring, electronegative groups around the benzamide

moiety and hydrophobic group to the D-ring of NS-187 are necessary to increase the Bcr-Abl activity. The robustness of the 3D-QSAR models constructed was validated by good predictive r^2 and consistency between the contour maps and docking analysis. The study provided insights into the ligand structural requirements to achieve better Bcr-Abl activity which can be utilized in the design of new and more potent Bcr-Abl agents.

Acknowledgements

The author acknowledges Dr. David Wild (Indiana University) for critically reading the manuscript and Prof. Jonathan Hirst (Nottingham University) for generously facilitating the publication. Special thanks to Mr. Berhane Gebru (Germany) whose enthusiasm and guidance made it possible to publish this paper.

References

- [1] M.W. Deininger, J.M. Goldman, J.V. Melo, The molecular biology of chronic myeloid leukemia, *Blood* 96 (2000) 3343–3356.
- [2] E. Buchdunger, A. Matter, B.J. Druker, Bcr-Abl inhibition as a modality of CML therapeutics, *Biochim. Biophys. Acta* 1551 (2001) M11–M18.
- [3] M.W.N. Deininger, B.J. Druker, Specific targeted therapy of chronic myelogenous leukemia with imatinib, *Pharmacol. Rev.* 55 (2003) 401–424.
- [4] R. Capdeville, E. Buchdunger, J. Zimmermann, A. Matter, Glivec (STI571, imatinib), a rationally developed, targeted anticancer drug, *Nat. Rev. Drug Discov.* 1 (2002) 493–502.
- [5] B.J. Druker, STI571 (Gleevec) as a paradigm for cancer therapy, *Trends Mol. Med.* 8 (4 Suppl.) (2002) S14–S18.
- [6] C. Sawyers, Targeted cancer therapy, *Nature (London)* 7015 (2004) 294–297.
- [7] T. Schindler, W. Bornmann, P. Pellicena, W.T. Miller, B. Clarkson, J. Kuriyan, Structural mechanism for STI571 inhibition of Abelson tyrosine kinase, *Science* 289 (2000) 1938–1941.
- [8] O. Hantschel, B. Nagar, S. Guettler, J. Kretschmar, K. Dorey, J. Kuriyan, G. Superti-Furga, A myristoyl/phosphotyrosine switch regulates c-Abl, *Cell* 112 (2003) 845–857.
- [9] B. Nagar, W.G. Bornmann, P. Pellicena, T. Schindler, D.R. Veach, W.T. Miller, B. Clarkson, J. Kuriyan, Crystal structures of the kinase domain of c-Abl in complex with the small molecule inhibitors PD173955 and imatinib (STI571), *Cancer Res.* 62 (2002) 4236–4243.
- [10] S. Wong, O.N. Witte, The BCR-ABL story: bench to bedside and back, *Annu. Rev. Immunol.* 22 (2004) 247–306.
- [11] S.W. Cowan-Jacob, V. Guez, G. Fendrich, J.D. Griffin, D. Fabbro, P. Furet, J. Liebetanz, J. Mestan, P.W. Manley, Imatinib (STI571) resistance in chronic myelogenous leukemia: molecular basis of the underlying mechanisms and potential strategies for treatment, *Mini-rev. Med. Chem.* 4 (2004) 285–299.
- [12] C. Roche-Lestienne, V. Soenen-Cornu, N. Grardel-Duflos, J.L. Lai, N. Philippe, T. Facon, P. Fenaux, C. Preudhomme, Several types of mutations of the Abl gene can be found in chronic myeloid leukemia patients resistant to STI571, and they can pre-exist to the onset of treatment, *Blood (New York)* 100 (2002) 1014–1018.
- [13] A. Hochhaus, S. Kreil, A. Corbin, S. La Rosee, P. Muller, M.C. Lahaye, T. Hanfstein, B. Schoch, C. Cross, N.C.U. Berger, Molecular and chromosomal mechanisms of resistance to imatinib (STI571) therapy, *Leukemia* 11 (2002) 2190–2196.
- [14] N. von Bubnoff, C. Peschel, J. Duyster, Resistance of Philadelphia-chromosome positive leukemia towards the kinase inhibitor imatinib (STI571, Glivec): a targeted oncoprotein strikes back, *Leukemia* 17 (2003) 829–838.

- [15] N.P. Shah, J.M. Nicoll, B. Nagar, M.E. Gorre, R.L. Paquette, J. Kuriyan, C.L. Sawyers, Multiple BCR-ABL kinase domain mutations confer polyclonal resistance to the tyrosine kinase inhibitor imatinib (STI571) in chronic phase and blast crisis chronic myeloid leukemia, *Cancer Cell* 2 (2002) 117–126.
- [16] S.W. Cowan-Jacob, G. Fendrich, A. Floersheimer, P. Furet, J. Liebetanz, G. Rummel, P. Rheinberger, M. Centeleghe, D. Fabbro, P.W. Manley, Structural biology contributions to the discovery of drugs to treat chronic myelogenous leukemia, *Acta Cryst. D* 63 (2007) 80–93.
- [17] M. Copland, A. Hamilton, L.J. Elrick, J.W. Baird, E.K. Allan, N. Jordanides, M. Barow, J.C. Mountford, T.L. Holyoake, Dasatinib, (BMS-354825) targets an earlier progenitor population than imatinib in primary CML but does not eliminate the quiescent fraction, *Blood* 107 (11) (2006) 4532–4539.
- [18] N.P. Shah, C. Tran, F.Y. Lee, P. Chen, D. Norris, C.L. Sawyers, Overriding imatinib resistance with a novel ABL kinase inhibitor, *Science* 305 (2004) 399–401.
- [19] P. La Rosee, A.S. Corbin, E.P. Stoffregen, M.W. Deininger, B. Druker, Activity of the Bcr-Abl kinase inhibitor PD180970 against clinically relevant Bcr-Abl isoforms that causes resistance to imatinib mesylate (Gleevec STI571), *Cancer Res.* 62 (2002) 7149–7153.
- [20] D. Wisniewski, C.L. Lambek, C. Liu, A. Strife, D.R. Veach, B. Nagar, M.A. Young, T. Schindler, W.G. Bornman, J.R. Bertino, J. Kuriyan, B. Clarkson, Characterization of potent inhibitors of the Bcr-Abl and the c-kit receptor tyrosine kinase, *Cancer Res.* 62 (2002) 4244–4255.
- [21] E. Weisberg, P.W. Manley, W. Breitenstein, J. Bruggen, S.W. Cowan-Jacob, A. Ray, B. Huntly, D. Fabbro, G. Fendrich, E. Hall-Meyers, A.L. Kung, J. Mestan, G.Q. Daley, L. Callahan, L. Catley, C. Cavazza, A. Mohammed, D. Neuberg, R.D. Wright, D.G. Gilliland, J.D. Griffin, Characterization of AMN107, a selective inhibitor of native and mutant Bcr-Abl, *Cancer Cell.* 7 (2005) 129–141.
- [22] E.A. Harrington, D. Bebbington, J. Moore, R.K. Rasmussen, A.O. Ajose-Adeogun, T. Nakayama, J.A. Graham, C. Demur, T. Hercend, A. Diu-Hercend, VX-680, a potent and selective small-molecule inhibitor of the Aurora kinases, suppresses tumor growth in vivo, *Nat. Med.* 10 (2004) 262–267.
- [23] J.F. Dorsey, R. Jove, A.J. Kraker, J. Wu, The pyrido [2,3-d] pyrimidine derivative PD180970 inhibits p210^{Bcr-Abl} tyrosine kinase and induces apoptosis of K562 leukemic cells, *Cancer Res.* 60 (2000) 3127–3131.
- [24] J. Zimmermann, E. Buchdunger, H. Mett, T. Meyer, N.B. Lydon, Potent and selective inhibitors of the Abl-kinase: phenylaminopyrimidine (PAP) derivatives, *Bioorg. Med. Chem. Lett.* 7 (1997) 187–192.
- [25] Z. Rachid, A. Katsoulas, F. Brahimi, B.J. Jean-Claude, Synthesis of pyrimidinopyridine-triazene conjugates targeted to Abl tyrosine kinase, *Bioorg. Med. Chem. Lett.* 13 (2003) 3297–3300.
- [26] P.W. Manley, W. Breitenstein, J. Bruggen, S.W. Cowan-Jacob, P. Furet, J. Mestan, T. Meyer, Urea derivatives of STI571 as inhibitors of Bcr-Abl and PDGFR kinases, *Bioorg. Med. Chem. Lett.* 14 (2004) 5793–5797.
- [27] T. Asaki, Y. Sugiyama, T. Hamamoto, M. Higashioka, M. Umehara, H. Naito, T. Niwa, Design and synthesis of 3-substituted benzamide derivatives as Bcr-Abl kinase inhibitors, *Bioorg. Med. Chem. Lett.* 16 (2006) 1421–1425.
- [28] B. Nagar, O. Hantschel, M.A. Young, K. Scheffzek, D. Veach, W. Bornmann, B. Clarkson, G. Superti-Furga, J. Kuriyan, Structural basis for the autoinhibition of c-Abl tyrosine kinase, *Cell* 112 (2003) 859–871.
- [29] SYBYL Version 7.2, Tripos Inc., 1699 South Hanley Road, St. Louis, MO 63144, USA, 2006.
- [30] M. Clark, R. Cramer III, N. Van Opdenbosch, Validation of the general purpose Tripos 5.2 force field, *J. Comput. Chem.* 10 (1989) 982–1012.
- [31] R.D. Cramer III, D.E. Patterson, J.D. Bunce, Comparative molecular field analysis (CoMFA) 1. Effect of shape on binding of steroids to carrier proteins, *J. Am. Chem. Soc.* 110 (1988) 5959–5967.
- [32] K. Kim, G. Greco, E. Novellino, A critical review of recent CoMFA applications, *Perspec. Drug Discov. Des.* 12–14 (1998) 257–315.
- [33] G. Klebe, U. Abraham, T. Mietzner, Molecular similarity indices in a comparative analysis (CoMSIA) of drug molecules to correlate and predict their biological activity, *J. Med. Chem.* 37 (1994) 4130–4146.
- [34] M. Bohm, J. Sturbecher, G. Klebe, Three-dimensional quantitative structure–activity relationship analyses using comparative molecular field analysis and comparative molecular similarity indices analysis to elucidate selectivity differences of inhibitors binding to trypsin, thrombin, and factor Xa, *J. Med. Chem.* 42 (1999) 458–477.
- [35] R. Cramer III, J. Bunce, D. Patterson, I. Frank, Crossvalidation, bootstrapping, and partial least squares compared with multiple regression in conventional QSAR studies, *Quant. Struct. Act. Relat.* 7 (1988) 18–25.
- [36] L. Stahle, S. Wold, Multivariate data analysis and experimental design in biomedical research, in: G.P. Ellis, G.B. West (Eds.), *Progress in Medicinal Chemistry*, Elsevier, Netherlands, 1988, pp. 292–338.
- [37] B. Bush, R. Nachbar, Sample-distance partial least squares: PLS optimized for many variables, with application to CoMFA, *J. Comput. Aided Mol. Des.* 7 (1993) 587–619.
- [38] A. Leach, V. Gillet, *An Introduction to Chemoinformatics*, Kluwer Academic Publisher, Dordrecht, United Kingdom, 2003.
- [39] W. Sippl, H. Höltje, Structure-based 3D-QSAR—merging the accuracy of structure-based alignments with the computational efficiency of ligand-based methods, *J. Mol. Struct. (Theochem.)* 503 (2000) 31–50.
- [40] J. Buolamwini, H. Assefa, CoMFA and CoMSIA 3D-QSAR and docking studies on conformationally-restrained cinnamoyl HIV-1 integrase inhibitors: exploration of a binding mode at the active site, *J. Med. Chem.* 45 (2002) 841–852.
- [41] G. Desiraju, B. Gopalakrishnan, R. Jetti, A. Nagaraju, D. Raveendra, J. Sarma, M. Sobhia, R. Thilagavathi, Computer-aided design of selective COX-2 inhibitors: comparative molecular field analysis, comparative molecular similarity indices analysis, and docking studies of some 1,2-diarylimidazole derivatives, *J. Med. Chem.* 45 (2002) 4847–4857.
- [42] M. Rarey, B. Kramer, T. Lengauer, G. Klebe, A fast flexible docking method using an incremental construction algorithm, *J. Mol. Biol.* 261 (1996) 470–489.
- [43] B. Kramer, M. Rarey, T. Lengauer, Evaluation of the FlexX incremental construction algorithm for protein–ligand docking, *Proteins: Struct. Funct. Gen.* 37 (1999) 228–241.
- [44] M. Young, N. Shah, L. Chao, M. Seeliger, Z. Milanov, W. Biggs, D. Treiber, H. Patel, P. Zarrinkar, D. Lockhart, C. Sawyers, J. Kuriyan, Structure of the kinase domain of an imatinib-resistant Abl mutant in complex with the Aurora kinase inhibitor VX-680, *Cancer Res.* 66 (2006) 1007–1014.
- [45] A. Tropsha, in: T. Oprea (Ed.), *Cheminformatics in Drug Discovery*, Wiley, Weinheim, 2005, p. 437.